INVESTIGATION OF TECHNOLOGICAL SIZE EFFECTS OF WELDING ON THE RESIDUAL STRESSES AND FATIGUE LIFE OF TUBULAR JOINTS MADE OF STRUCTURAL STEELS S355 AND S690

Farshid Zamiri[a], Claire Acevedo[a], Alain Nussbaumer[a], Janna Krummenacker[b]

[a] École Polytechnique Fédérale de Lausanne (EPFL), Switzerland
[b] Karlsruhe Institute of Technology (KIT), Germany

Abstract. The fabrication procedure changes when changing the size of the structural components. For the weldments, the change of the welding procedure leads to the change in residual stresses which consequently affects the fatigue life of the structure. The weld size and number of welding passes are important factors which have considerable impact on the values and distribution of the welding residual stresses. This technological size effect is investigated in this study by simulating the welding process for tubular joints made of S355 and S690 structural steel. Two types of joints are studied: circumferential weld and planar K-joint.
While rapidly developing, coupled thermo-mechanical analysis of welding is a powerful and versatile tool for the study of the development of thermal strains and stresses cause by welding process. In this study, both multi-pass and single-pass procedures with their corresponding simulation parameters are investigated. The resulted residual stress field when superposed into applied stresses at the joint in a crack propagation analysis yield more realistic crack pass and crack propagation life estimation.

1 INTRODUCTION

As it is observed in numerous experiments, the fatigue strength of the welded details is size dependent. The fatigue life of a larger joint with thicker plate(s) is smaller than fatigue life of a thinner joint with similar geometry and under similar nominal stress [1]. Therefore, part of the fatigue strength gain that potentially can be achieved in a detail by increasing the thickness of the elements is lost due to the detrimental size effect.
The current size effect provisions in CIDECT [2] and IIW [3] codes are largely based on a statistical study of a large database of fatigue tests expressed as hot spot stress results for tubular joints carried out by van Wingerde and his colleagues [4]. The proposed relation is as follows:

$$\frac{S_{r,hs,T}}{S_{r,hs,Tref}} = \left(\frac{T_{ref}}{T}\right)^{n} \qquad (1)$$

Where $S_{r,hs,T}$ is the hot-spot fatigue strength of the tubular joint with thickness T , T_{ref} is reference thickness (16 mm), and n is the size correction coefficient which is proposed as a function of fatigue life and varies between 0.24 (for 10^4 cycles) to 0.402 (for 5×10^6 cycles). For the case of non-proportional scaling of welded K-joints, Borges [5] has proposed size effect relations that in addition to the thickness, take into consideration some additional geometric parameters of the detail, including chord slenderness $\gamma = D/(2T)$, brace to chord thickness ratio $\tau = t/T$, and diameter ratio $\beta = d/D$. Non-proportional scaling as described by [6], is the case when the geometric features of the two details are not scaled by the same ratio.
Three factors are considered to contribute to the size effect ([4], [6], and [7]):

- *Geometrical size effect*: stress gradient at the vicinity of the crack site will be different when the size changes. A small surface crack, such as the one shown on plate T_2 in Figure 1, experiences a higher stress value than the similar crack on the thinner plate T_1 , because of the lower stress gradient existing in the plate T_2 . This will result in smaller fatigue life for the plate T_2 compared to T_1 despite their equal nominal stress value.
- *Statistical size effect*: The probability of existence of defects (cracking sites) increases with the increase of the size of the element,

Technological size effect: Differences in production procedures can contribute to the change in the fatigue life of the structures with different scales. This can be due to the metallurgical (microstructure) change, change in the surface roughness, or due to residual stresses. The change in the welding procedure (weld size, welding sequence, and number of welding passes) will alter the distribution of residual stresses in the critical sections. Welding residual stresses can be as high as the yield strength of the metal [8].Tensile residual stresses will tend to keep the cracks open during all or part of the load cycle, which will be detrimental to the fatigue life of the detail.

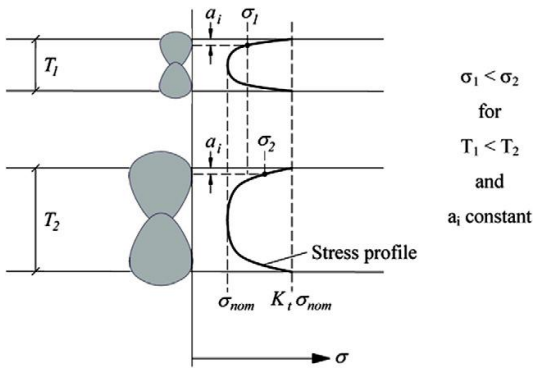

Figure 1. Geometrical size effect [9].

1.1 Welding simulation

During the process of fusion welding, a lot of interactions occur between three major fields ([10], [11]): Thermal field, mechanical field, and microstructure field. A simplified diagram which shows some more significant interactions is presented in Figure 2. The dark arrows show the dominating effects and the dotted arrows indicate the effects of less importance. The temperature field affects both the residual stress field and the microstructure field, but the inverse effects can be neglected most of the time. This helps the de-coupling of the thermo-mechanical analysis into a sequential procedure of solving the heat conduction problem, followed by a mechanical analysis.

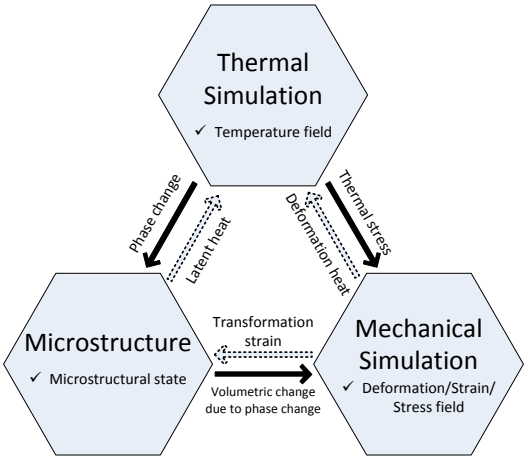

Figure 2. Subdomains of welding simulation with important interactions. Adapted from [10].

The original steel composition and the thermal cycle which the material undergoes, determine the phase transformations and final microstructure of the weld and heat affected zone [10]. When heated up to welding temperature, steel transforms into austenite and during the cooling down, austenite can transform into martensite (rapid cooling), bainite (medium-rate cooling), or ferrite-pearlite (slow cooling). Martensite is a brittle structure and its low fracture toughness can affect the fatigue life of the welded detail. The volume change also happens due to the phase transformation which will lead to extra residual stresses. The influence of volumetric change caused by phase transformation is studied by Lee and Chang [12] in their simulations of girth welds of high strength steel pipes.

2 GIRTH WELD

2.1 Model description

In order to assess the effect of number of welding passes on the residual stress field, a preliminary study was conducted on the circumferential butt welds of two tube sections with the same size. The girth weld of two ROR193.4x20 tube sections is simulated with two different methods: an equivalent single-pass welding and a three-pass welding. The ends of both tubes are beveled with an angle of 30° to form the weld gap.

2.1.1 Material data:

Temperature-dependent thermal material properties (thermal conductivity and specific heat capacity) are selected according to Eurocode 3 recommendations for structural fire design [13]. For the mechanical properties, yield

strength and modulus of elasticity of the constructional steels S355 and S690 at elevated temperatures were determined by a number of tests [14]. The values obtained during the tests were in good agreement with EC3 recommendations. The coefficient of thermal expansion was not measured during this experiments but a comparison was made between experimental data reported by Wichers [15] and Eurocode values (Figure 3a) which showed to be in agreement. For the analyses presented here, the curves from the EC3 recommendations (shown in Figure 3) were chosen for the yield strength, modulus of elasticity, and coefficient of thermal expansion. The same material properties are assumed for the parent metal and weld material. The volumetric changes due to phase transformation are not considered in this stage of study.

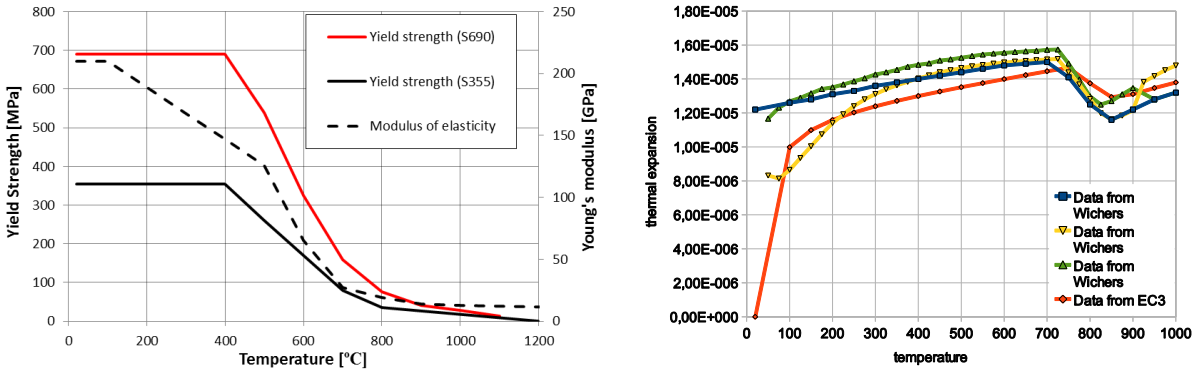

(a) (b)

Figure 3. Material data used in analyses (a) Modulus of elasticity and Yield strength diagrams according to [13]; (b) Comparison of steel thermal expansion coefficient given in Eurocode [13] and values measured by [15].

2.1.2 Heat source and boundary conditions

Simplifications have been recommended in the literature to facilitate the simulation of the complex processes which take place in the weld pool ([10], [16–18]). The processes inside the molten zone (e.g. material movement and internal convection within the weld pool) are not considered in the simulation. The important characteristics of the heat source used in the analyses are summarized in Table I. The moving heat source was modelled using a DFLUX user subroutine in ABAQUS finite element analysis program [19]. The same value was used for the total heat input in both the equivalent single pass and the three pass welding simulations. As shown in Figure 4, the shape of the heat source is considered hemispherical (in the case of single-pass model) or spherical (in the case of multi-pass model) with uniform heat input intensity. The size of the hemispherical heat source for single-pass weld was selected such that the size of molten area be consistent with weld gap size. The total volume spherical heat sources of three-pass welding were chosen to be equal to the hemisphere in the single-pass model. It should be noted that Goldak's double ellipsoid weld shape provides a more accurate representation of the heat source [11], but its calibration requires more experimental data.

Table I. Heat source specifications for single pass and multipass modeling of the girth weld.

	Single pass	Multi pass
Heat power input [kW]	13.8	3.4 (pass1) + 5.2 (pass2) + 5.2 (pass3)
Volumetric heat input [W/mm^3]	5	5
Welding speed [cm/min]	90	90
Interpass delay [sec] *	-	300

* The interpass temperature was checked to be below 200°C which was prescribed by welding procedure specifications.

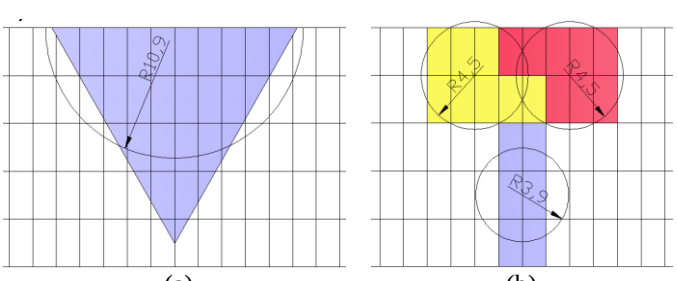

(a) (b)

Figure 4. Shape of the heat source (a) single-pass and (b) multi-pass weld simulations. The shaded area in (a) represents the weld gap shape.

The convection follows Newton's law and for the radiation the standard Boltzmann relation can be applied. The emissivity and convective heat transfer coefficient values suggested by Brown and Song were used [20]. In order to model radiation and convection heat transfer in ABAQUS, a combined film coefficient was used in the *FILM block of the input file.

2.1.3 Finite element models

The computation domain is discretised to 60'000 eight-node isoperimetric solid elements (C3D8R). The mesh size is 2mm*2mm (on tube surface) and 4mm (in the thickness direction) in the region close to the weld line. The mesh size is increased in the other regions to save the computation time. The element birth or element activation technique can be used to model the weld metal deposition in the multi-pass welding simulations. The technique is more tedious to implement in the welding simulation using ABAQUS compared to some other packages (e.g. ANSYS) and was not applied in this study. Figure 5 shows part of the FE model and a snapshot of the temperature field results. When a new weld pass is deposited, the regions which are heated to temperatures around 800°C and above will plastify and hence their existing residual stresses are erased. This is implemented in the model by passing an annealing command to the program at the beginning of each weld pass, which sets the residual stress state to zero.

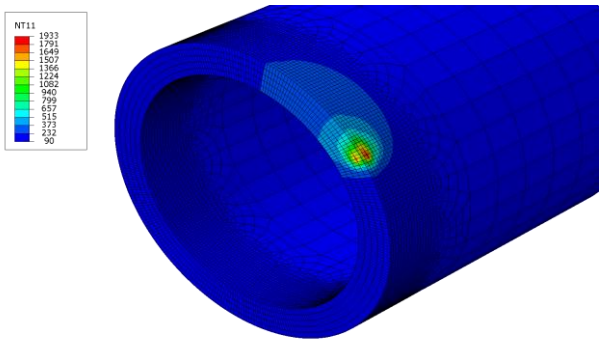

Figure 5. Temperature field resulted from the moving heat source. Half of the model is shown for clarity.

2.2 Results

The axial and hoop components of residual stress profiles at the weld toe are presented in Figure 6 together with the SINTAP profiles [8] for the two steel grades. For each simulation type (single-pass, multi-pass), two profiles are presented: one for the weld start-stop point (location 0°), and one point at the mid-path of the weld line (location 180°).

The trend and shape of the profiles resulted from multi-pass simulation is in general agreement with SINTAP curves published by Stacey and his colleagues [8]. One significant deviation from Stacey's predictions is the axial stress component in the inner surface of the tube which needs more investigation in the subsequent studies. For the points located on the tube surface, The SINTAP curves report higher tensile stresses than our analysis results. They also overestimate the compressive residual stresses on the outer surface of the tube, e.g. at $z/T=0$ in Figure 6.(a) and (c). For the fatigue life of the detail, this could potentially reduce the fatigue life, since the stress cycles in those locations might become partially tensional.

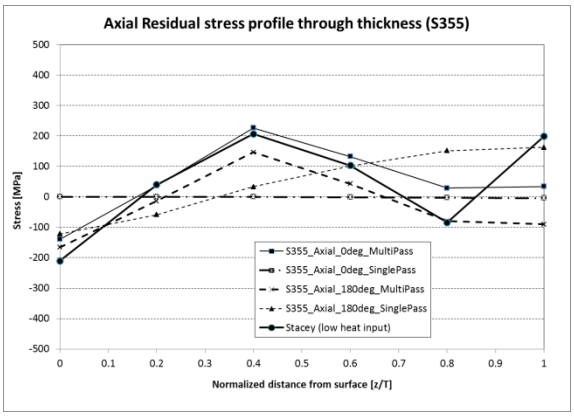

(a)

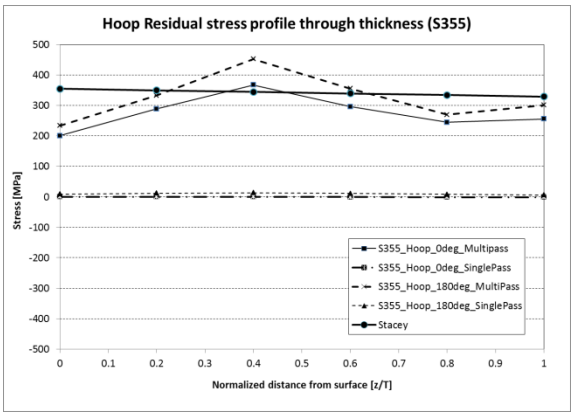

(b)

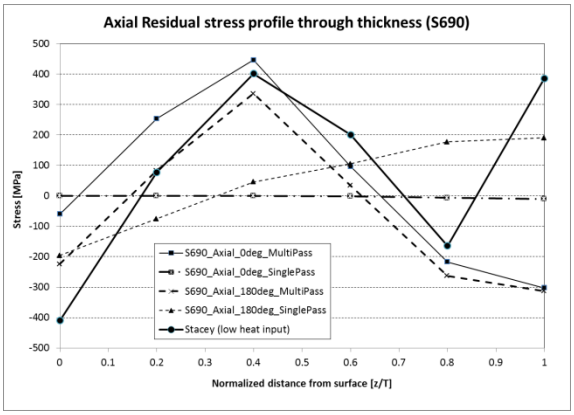

(c)

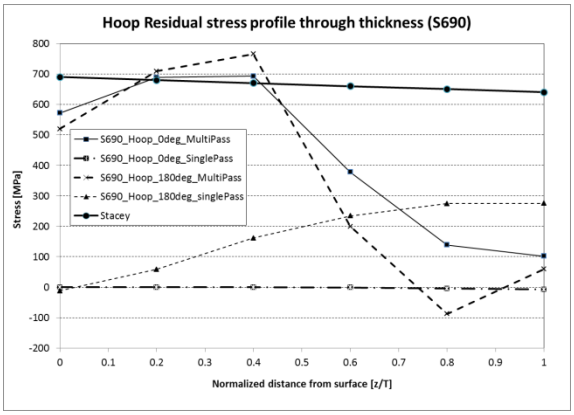

(d)

Figure 6. Residual stress profiles for the tube joint; (a) axial stress-S355 steel; (b) hoop stress-S355 steel; (c) axial stress-S690 steel; (d) hoop stress-S690 steel.

3 WELDED TUBULAR K-JOINT

3.1 Thermo-mechanical simulation

Full scale fatigue tests of tubular trusses have shown that the tensile residual stresses significantly change the fatigue response of the details loaded in compression by keeping the cracks open for all or part of the load cycles [21]. The geometry and loading for the K-joint modelled here is similar to the joint available in the aforementioned tests. A summary of nominal member sizes and non-dimensional geometric features of the joint is presented in Table II. The material properties for S355 where chosen similar to the case of circumferential butt joint (See paragraph 2.1.1).

MORFEO[1] finite element code was used for the thermo-mechanical simulation of the welding [22]. MORFEO is not a general finite element package like ABAQUS, but rather it is dedicated to simulation of the manufacturing processes such as machining, welding. The definition of heat source and its trajectory is more straightforward in MORFEO. The solver algorithms in MORFEO are also optimized to gain the minimal computation time for thermo-mechanical analyses.

Table II. Welded CHS K-joint dimensions and non-dimensional parameters.

Nominal dimensions [mm]		Non dimensional parameters	
Chord	168.3×20	β (d/D)	0.53
Brace	88.9×8	γ (D/2T)	4.21
θ *	60°	τ (t/T)	0.4

* Nominal angle between the chord and braces

The specifications of the heat source (weld torch) are presented in Table III. The real welding procedure consisted of 7 passes. These passes were combined into a single equivalent pass. During the welding in the workshop, the two circular weld line of the joint were divided into smaller passes and were welded according the sequence shown in Table IV. This sequence was applied in the simulation as well. Table IV also contains the timing information for this welding sequence. The heat source was selected in the shape of a frustum of a cone with uniform intensity for the heat input. The radii of the bases of the cone were r_1=15mm and r_2=9.3mm and the height of the cone was h=15mm. The heat source dimensions were selected to fit within the measured weld pool size.

A convergence study was performed to check if the refinement in the mesh is adequate. The mesh size in the gap region is smaller in the outer surface of the tube to provide a better resolution for study of the residual stresses at the region where the cracking starts. Figure 7 shows the finite element mesh used in the analysis. The colors in the figure represent a snapshot of the temperature field solution. 8-node brick elements with 8 Gauss points (i.e. no reduced integration) are used in the analysis. For the thermal analysis, these elements seem to be most computationally cost effective elements which also provide good accuracy. Thermal analysis is by far the most computation intensive part of the analysis.

[1] MORFEO: Manufacturing ORiented Finite Element tOol

3.2 Residual stress results

The components of the residual stress field resulted from the thermo-mechanical welding is shown on a cut section of the K-joint in Figure 8 for the case of steel grade S355. Figure 9 presents the through thickness profiles of the three compoinents (longitudinal, trnaverse and radial directions) in the chords at the brace-to-chord weld toes. The profiles show considerable difference in residual stresses between the right and left brace locations which is attributed to the welding sequence of the detail.

Table III. Heat source specifications for CHS K-joint.

	Single pass
Welding current [A]	270
Voltage [U]	30
Arc welding efficiency [%]	0.732
Heat power input [kW]	13.8
Heat input [kW]	41.5
Volumetric heat input [W/mm^3]	5.87

Table IV. Welding sequence and start/stop times for thermal analysis of single pass weld

Step name	Start time [s]	End time [s]
Waiting step	0	24
Welding, path 1	25	50
Cooling	51	174
Welding, path 2	175	200
Cooling	201	324
Welding, path 3	325	350
Cooling	351	474
Welding, path 4	475	500
Cooling	501	9501

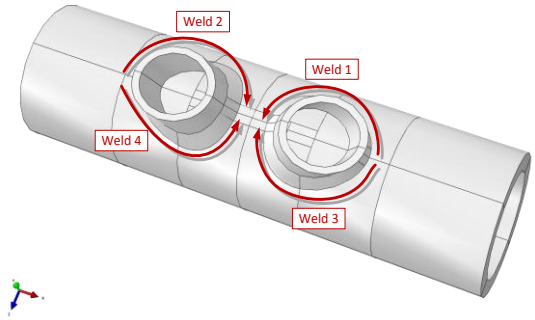

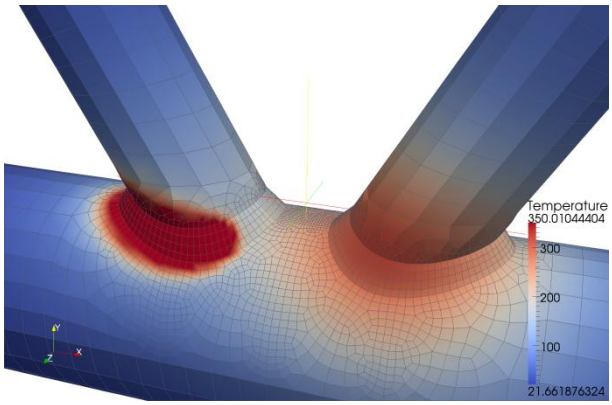

Figure 7. Temperature field during the welding. Equivalent single pass model

The highest tensile residual stresses occur at the gap region in the K-joint in the transverse direction to the weld (i.e. the component which is paralle to the chord axis). This high level of stresses called restraining effect occuring in the gap region of the joint is discussed in more detail in [21]. The transverse stress component is in the same direction as stresses from axial loading and in-plane bending and will contribute to mode I fatigue cracking. As can be seen in the stress profiles the magnitude of the transverse stresses is equal to, and even higher than the yield strength of the steel (for both S355 and S690 grades). Therefore, it is expected that the cracks will remain open, even in a region with compressive applied stresses, for all of the loading cycle.

The resulted residual stress field from the thermo-mechanical welding can be superposed with the applied stresses in a crack propagation analysis conducted in the extended finite element (XFEM) code MORFEO-Crack.

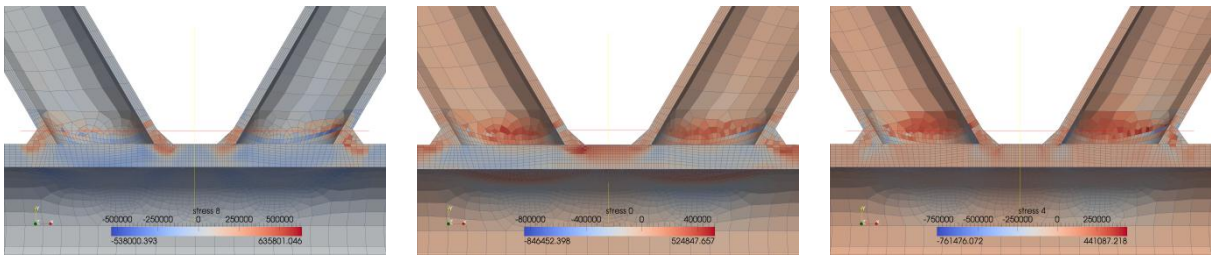

(a) (b) (c)

Figure 8. Residual stresses at the K-joint (S355 Steel). Equivalent single pass model (a) Transverse component; (b) Longitudinal component; (c) Radial component.

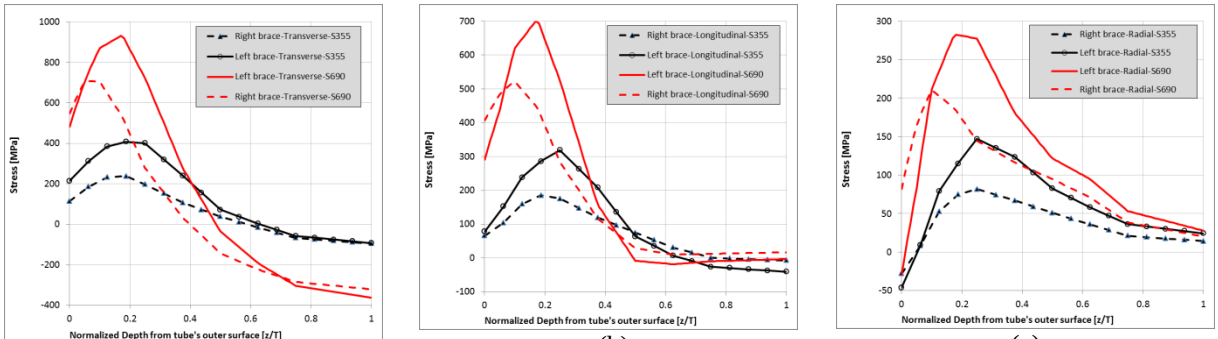

(a) (b) (c)

Figure 9. Residual stress profiles through thickness at the weld toes in the location of right and left braces; (a) Transverse component (parallel to the chord axis); (b) Longitudinal component; (c) Radial component.

4 CONCLUSIONS

Thermo-mechanical welding analysis was applied to determine the welding residual stresses in a welded tubular circumferential joint and a planar K-joint with different steel grades (S355 and S690).

The simulation results for the circumferential weld show that the axial residual stress profiles shape remain unchanged (although the stress values change) when changing the steel grade from S355 to S690. However, this may not be the case when including the volumetric strains caused by the phase transformation in high strength steel.

For the case of planar K-joint, again the shapes of the residual stress curves for the two steel grades S355 and S690 are similar. This might change when the volumetric changes due to the phase transformation effects will be implemented in the models. Although the K-joint geometry is symmetric, the asymmetry in the residual stress field is observed due to the welding sequence selected. This suggests for more detailed study of the effect of welding sequence on the residual stress state in the planar K-joint by the thermo-mechanical welding simulation tool. The asymmetry is less significant for the S690 steel. The residual stress profiles show high tensile stresses at the outer surface of the chord in the direction of chord axis which is in agreement with the fatigue cracking observed in the previous full-scale fatigue tests [21].

For an improved crack propagation life assessment, the residual stress field can be added to the applied stresses in the joint in a crack propagation analysis with the XFEM analysis tools such as MORFEO-Crack.

5 REFERENCES

1. T. R. Gurney, The influence of thickness on the fatigue strength of welded joints, in *Proceedings of the Second International Conference on the Behaviour of Off-Shore Structures, held at Imperial College, London, England*, 1979.
2. X. L. Zhao, S. Herion, and J. A. Packer, CIDECT Design Guide 8—Design guide for circular and rectangular hollow section joints under fatigue loading, *Cologne: CIDECT*, 2001.
3. A. Hobbacher, Recommendations for Fatigue Design of Welded Joints and Components IIW Document XIII-1965-03, XV-1127-03, Paris, 2003.
4. A. M. Van Wingerde, D. R. V. Van Delft, J. Wardenier, and J. A. Packer, Scale effects on the fatigue behaviour of tubular structures, in *WRC Proceedings IIW*, San Francisco, 1997, pp. 123-135.
5. L. A. Costa Borges, Size effects in the fatigue behaviour of tubular bridge joints, EPFL, Lausanne, 2008.
6. F. R. Mashiri, X. L. Zhao, M. A. Hirt, and A. Nussbaumer, Size effect of welded thin-walled tubular joints, *International Journal of Structural Stability and Dynamics*, vol. 7, no. 1, pp. 101-127, 2007.

7. E. Niemi and G. Marquis, Introduction to the structural stress approach to fatigue analysis of plate structures, in *Proceedings of the IIW fatigue seminar*, 2002, pp. 73–90.
8. A. Stacey, J.-Y. Barthelemy, R. H. Leggatt, and R. A. Ainsworth, Incorporation of residual stresses into the SINTAP defect assessment procedure, *Engineering Fracture Mechanics*, vol. 67, no. 6, pp. 573-611, 2000.
9. A. Schumacher, L. C. Borges, and A. Nussbaumer, A critical examination of the size effect correction for welded steel tubular joints, *International Journal of Fatigue*, vol. 31, no. 8-9, pp. 1422-1433, 2009.
10. D. Radaj, *Welding residual stresses and distortion*. DVS - Verlag, 2003.
11. J. A. Goldak and M. Akhlaghi, *Computational welding mechanics*. Springer Verlag, 2005.
12. C. H. Lee and K. H. Chang, Prediction of residual stresses in high strength carbon steel pipe weld considering solid-state phase transformation effects, *Computers & Structures*, 2010.
13. EN1993, *Eurocode 3: Design of steel structures - Part 1-2:General rules - Structural fire design*. Brussels: European Committee for Standardization, 2005.
14. J. Krummenacker, Simulation of the welding process of steel tube joints made of S355 and S690, Karlsruher Institut für Technologie/École Polytechnic Fédérale de Lausanne, 2011.
15. M. Wichers, Schweißen unter einachsiger, zyklischer Beanspruchung Experimentelle und numerische Untersuchungen(Welding under uniaxial cyclic loads – Experimental and numerical research), Universitätsbibliothek Braunschweig, 2006.
16. L.-E. Lindgren, Finite element modeling and simulation of welding part 1: Increased complexity, *Journal of Thermal Stresses*, vol. 24, no. 2, pp. 141-192, 2001.
17. L. E. Lindgren, Finite element modeling and simulation of welding. part 2: Improved material modeling, *Journal of thermal stresses*, vol. 24, no. 3, pp. 195-231, 2001.
18. L.-E. Lindgren, "Finite element modeling and simulation of welding. Part 3: Efficiency and integration, *Journal of Thermal Stresses*, vol. 24, no. 4, pp. 305-334, 2001.
19. ABAQUS, Inc., *ABAQUS Analysis: User's Manual, Version 6.10*. Dassault systèmes., 2010.
20. S. Brown and H. Song, Finite element simulation of welding of large structures, *Journal of engineering for industry*, vol. 114, no. 4, pp. 441-451, 1992.
21. C. Acevedo, Influence of Residual Stresses on Fatigue Response of Welded Tubular Joints, EPFL, Lausanne, 2011.
22. MORFEO, MORFEO v1.5.2 User's Manual, Cenaero, 2011.